A new synthetic approach for substitutional solid solutions in a 3D coordination polymer: Cation vacancy, and tu...

Aliyu M. Hamisu

A new synthetic approach for substitutional solid solutions in a 3D coordination polymer: Cation vacancy, and tunable photoluminescence

Journal of Solid State Chemistry 279 (2019) 120948

Contents lists available at ScienceDirect

Journal of Solid State Chemistry

journal homepage: www.elsevier.com/locate/jssc

A new synthetic approach for substitutional solid solutions in a 3D coordination polymer: Cation vacancy, and tunable photoluminescence

Aliyu M. Hamisu [a], Fendi Y. Wardana [a], Azhar Ariffin [a], Irshad Baig [b], Christos D. Malliakas [c,**], Arief C. Wibowo [d,*]

[a] Department of Chemistry, University of Malaya, Kuala Lumpur, 50603, Malaysia
[b] Department of Chemistry, King Fahd University of Petroleum and Minerals, Dhahran, 31261, Saudi Arabia
[c] Department of Chemistry, Northwestern University, Evanston, IL, 60208, United States
[d] Department of Chemistry, University of Airlangga, Surabaya, East Java, 60115, Indonesia

ARTICLE INFO

Keywords:
Solid solution
Doped metal organic coordination polymer
Hetero-valent
Cation vacancy
Photoluminescence

ABSTRACT

Solid solution featuring mixed valence in metal-organic coordination polymer (MOCP) is rare. Inspired by the flexibility of Pb^{2+} to undergo cation exchange, and its ability to adopt a variety of coordination numbers (CN) and chemical environments (CE), herein we report the first, to our knowledge, hetero-valent, single and multiple substituted MOCP with cation vacancy featuring tunable photoluminescence, which may pave a way towards a tunable, functional MOCP. The 3D Pb MOCP features 1D moiety which contains three unique Pb^{2+} sites, each with a different CN and CE, that can undergo cationic substitutions with exogenous divalent as well as aliovalent, e.g. mono- or trivalent cations under appropriate conditions. The formation of solid solution is confirmed by Single Crystal and Powder X-ray Diffractions, SEM-EDS, ICP-OES, as well as XPS. A tunable photoluminescent (PL) color exhibiting good antennae effect and retention of original 3D Pb host color is observed using as little as 6 wt% of Eu^{3+} dopant. More importantly, the PL intensity of Eu^{3+} substituted Pb MOCP increases as dopant amount increases even up to 80 wt% doping, a rather rare case and the first, to our knowledge, in MOCP solid solution.

1. Introduction

Tunable physical or chemical functionalities in metal organic coordination polymers (MOCPs), can be ascribed largely to its tailorable chemical composition, flexibility, modular chemistry, high porosity or surface area. The tunable functionalities enable a target application by design, such as tunable light emission [1–4], luminescence sensors [3,5–7], energy [8], decontamination of pollutants via adsorption interactions [9–14]. In addition, the presence of defects in MOCPs and systematic understanding of their nature yield impressive benefits in controlling and manipulating their properties [15–20].

Defect engineering, through judicious control of structural defects and any related heterogeneity, is of unparalleled importance in solid state electronic materials, such as silicon, Group III/V semiconductor and its derivatives [21,22]. Application of such concept in metal-organic framework (MOF) or MOCP in general [15–17,20,23–36], would realize MOF with tunable properties [18,37]. Despite being an exciting concept to manipulate the structure and the resulting electronic properties, defect engineering by design in MOCP remains elusive [38–45]. In fact, based on recent reviews, it is reported that there is no well-documented report on MOCP with fully characterized cation vacancy due to partial replacement of cationic host by aliovalent cationic guest [18,19,27].

Compounds that contain main group element with lone pair are reported to be tolerant to defects [46–48], that can also be easily ion exchanged. Among frequently used cations for ion exchange in MOCP, Pb^{2+} possesses lowest electronegativity that gives labile ionic bonds, which in turn allowing it to be exchanged faster [49]. In addition, Pb^{2+} is one of the cations that are in borderline of Hard-Soft-Acid-Base (HSAB) concept [50,51], hence can adopt a variety of CE [52,53], in addition to having flexible CN (2-10) due to its large size [54–57]. Such features motivate us to search for a Pb MOCP system having more than one cation centres with different CN and CE from which each can undergo aliovalent cationic substitution to realize mixed valent, hence cation vacancy creation, and multiple doping.

The search narrows down to our previously synthesized 1D Pb MOCP

* Corresponding author.
** Corresponding author.
E-mail addresses: c-malliakas@northwestern.edu (C.D. Malliakas), wibowor@gmail.com (A.C. Wibowo).

https://doi.org/10.1016/j.jssc.2019.120948
Received 14 July 2019; Received in revised form 29 August 2019; Accepted 6 September 2019
Available online 11 September 2019

system that undergoes structural transformation into 3D MOCP that has three Pb^{2+} crystallographic sites with different CN and CE, fulfilling the pre-requisites, Fig. 1 [58]. Using such system, herein we report a successful synthesis of single and multiple doped MOCPs featuring hetero-valences and cation vacancy, as our first step towards defect engineering by design. Lithium substituted Pb^{2+} MOCP (*Li^{+}/Pb*) is synthesized to demonstrate monovalent substitution. Divalent cation substituted Pb^{2+} MOCPs (*M^{2+}/Pb*) featuring a variety of substituent's ionic radii (0.65–0.95 Å) are successfully synthesized. Lanthanide (Ln^{3+}) substituted Pb^{2+} MOCPs (*Ln^{3+}/Pb*) with cation vacancy are also successfully made featuring good antennae effect while preserving the 3D Pb host's original luminescent color, giving a dual color luminescence, with dopant amount as little as 6 wt%. Notably, an increased dopant, up to 80 wt%, with increased PL intensity is observed in Eu^{3+} doped Pb MOCP.

Further, a proof-of-concept compound is successfully orchestrated, proving the ability of this system to accommodate both divalent and trivalent exogenous cation dopants simultaneously, realizing, to our knowledge, the first multiple substituted, hetero-valent solid solution MOCP (*M^{2+}/M^{3+}/Pb*) with cation vacancy.

2. Experimental section

All reagents were purchased from Sigma-Aldrich and used without further purification. Semi-Quantitative analyses (atomic percentage of elements) were performed using Hitachi SU8220 Scanning Electron Microscope-Energy Dispersive Spectrometry (SEM-EDS) using washed and dried samples. *Li^{+}/Pb* and some *M^{3+}/Pb* stoichiometric ratio were determined using an analytikjena PlasmaQuant PQ 9000 Inductively Coupled Plasma-Optical Emission Spectroscopy (ICP-OES) spectrometry, using a washed and dried sample. Solid state photoluminescence measurements were performed using a Horiba LabRam Evolution high-resolution confocal Raman microscope spectrometer (600 g/mm diffraction grating) equipped with a diode continuous wave laser (473 nm, 25 mW) and a Synapse charge-coupled device camera. The maximum power output of the laser source was filtered to 1% of the maximum power output. Variation of dopant amount samples were measured using Edinburgh Instrument (FLS920). The solid state UV–Vis was carried out using diffuse reflectance PerkinElmer Lambda 950.

2.1. Synthesis of Pb-host, $Pb_2Cl_2(Hpzdc)_2(H_2O)_2$

A similar synthesis procedure reported by us [58,59] with further optimizations was adopted. Based on the new optimized method, the onset of the crystal formation time was greatly reduced to almost immediately, the clear solution was filtered and crystallization proceeded to completion within two to 3 h. A mixture of PbO (0.089 g, 0.4 mmol), H_2pzdc (0.067 g, 0.4 mmol), and piperazine (0.0215 g, 0.25 mmol) in DI water (20 ml) was heated and stirred at 70 °C. Subsequently, 10 drops of conc. HCl was added dropwise into the mixture resulting in a clear solution. The stirring and heating were continued for 5 min. Large, colorless, ribbon crystals were obtained in a quantitative yield after 2–3 h of slow evaporation. The final products were isolated by vacuum filtration, and dried at room temperature.

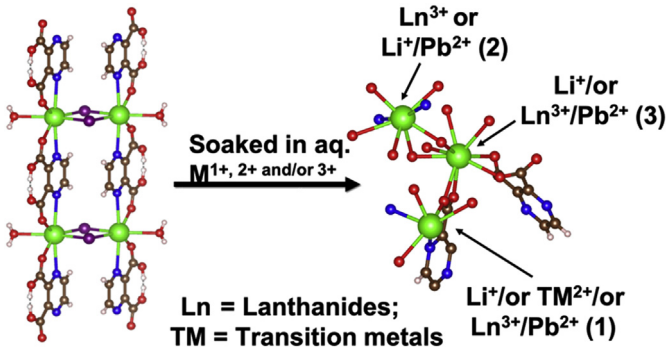

Fig. 1. Structural transformation from 1D into 3D featuring multiple doping and hetero-valences in Pb-based MOCP.

2.2. Synthesis of Li^{+}/Pb doped MOCP

Pb host (0.03 g, 0.035 mmol) was immersed into a ~7 ml aqueous solution of different Li(I)X precursor, X = NO_3, CH_3COO, OH, I, and PF_6 (0.066 mmol). The dissolution-recrystallization progress was examined in-situ under an optical microscope as a function of soaking time at room temperature. The obtained products with nearly quantitative yield (after 3d of soaking) were then washed thoroughly with fresh DI water and dried at room temperature prior to further characterizations. A quantitative analysis was performed by ICP-OES on some selected compounds.

2.3. Synthesis of M^{2+}/Pb doped product

Pb host (0.03 g, 0.035 mmol) was immersed into a ~7 ml aqueous solution of either nitrate and/or chloride precursor of M^{2+}, M = Co, Ni, Zn, or Cd (0.066 mmol). Washing and characterizations procedures were done similar to those of monovalent soaking. A semi-quantitative analysis was performed by SEM-EDS. The products were collected after 3d of soaking with nearly quantitative yield.

2.4. Rendering cation-exchanged product into a doped product

Cation-exchanged product was produced when Pb host (0.03 g, 0.035 mmol) was immersed into a ~7 ml aqueous solution of $FeCl_2$ or $CuCl_2$ (0.066 mmol). Rendering this into a doped product was successfully done by soaking Pb host (0.03 g, 0.035 mmol) into a ~7 ml DMF/H_2O (1:1) solution of $FeCl_2$ (0.066 mmol) or a ~7 ml DMF/H_2O/1,4-dioxane (1:1:1) solution of Copper (II) acetate (0.066 mmol). Washing and characterizations procedures were done similar to those of divalent soaking. The products were collected in quantitative yields after 3d of soaking.

2.5. Synthesis of M^{3+}/Pb doped product

Pb host (0.03 g, 0.035 mmol) was immersed into a ~7 ml aqueous solution of nitrate precursor of Ln^{3+}, Ln = La, Eu, Gd, Tb, or Er (0.066 mmol). Washing and characterizations procedures were done similar to those of divalent soaking. The products were collected in quantitative yields after 3d of soaking.

2.6. Synthesis of M^{3+}/Pb (M = Eu, Tb) with dopant variations

Pb host (0.03 g, 0.035 mmol) was immersed into a: ~7 ml aqueous solution, for condition (1) or ~7 ml H_2O/Dioxane/DMF mixture with the addition of 2 drops of pyridine, for condition (2) or same as (2) but with heating at 60 °C for 24 h, for condition (3), of nitrate precursor of Ln^{3+}, Ln = Eu or Tb (0.066 mmol). Washing and characterizations procedures were done similar to those of divalent soaking. All products were collected in quantitative yields after 3d of soaking, except for condition (3).

2.7. Synthesis of M^{3+}/M^{2+}/Pb doped product

Pb host (0.03 g, 0.035 mmol) was immersed into a ~7 ml aqueous solution of nitrate precursors of a mixture of Eu^{3+} (0.035 mmol) and Zn^{2+} (0.035 mmol). Washing and characterizations procedures were done similar to those of divalent soaking. The products were collected in quantitative yields after 3d of soaking.

2.8. Soaking 3D Pb MOCP in a solution of divalent cation precursor at room temperature

The 3D Pb MOCP, $Pb_3(pzdc)_3(H_2O)$, was synthesized according to the literature [59]. The resulting product (0.03 g, 0.035 mmol) was immersed into a ~7 ml aqueous solution of either nitrate and/or chloride precursor of Co^{2+} (0.066 mmol). The dissolution-recrystallization progress was examined in-situ under an optical microscope as a function of soaking time at room temperature. Two batches of products (after 3d and nearly 1 month of soaking) were then washed thoroughly with fresh DI water and dried at room temperature prior to further characterizations. A semi-quantitative analysis was performed by SEM-EDS.

2.9. X-ray Crystallography

Single crystal X-ray diffraction was performed on a Bruker Kappa APEX2 diffractometer with a MoKα (λ = 0.71073 Å) IμS microfocus source at 100 K. Prior to data collections, the single crystal samples were stored in a small amount of corresponding mother liquor in which each dissolution-recrystallization occurred. Data collection, cell refinement, and data reduction were carried out using the program APEX3 [60]. Numerical absorption corrections were performed with the program SADABS. Using Olex2 [61], the structure was solved with the ShelXS [62] structure solution program using Direct Methods and refined with the XL (Sheldrick, 2008) [62] refinement package using Least Squares minimization.

Most of the crystallographic contrast between the substituent and the Pb atoms sharing the same site comes from the refinement of the partial occupancy factor of the Pb atoms. Since the atomic structure factor of Pb is very large, determination of the partial occupancy of Pb is very sensitive to the amount of substitution. As the substituted members are semiconductors, all crystallographic refinements were performed assuming charge balance. Therefore, a soft constrain (SUMP command) was used for imposing charge balance for all atoms that occupy partially the Pb sites. Because the valence state of most substituents is different (aliovalent) than that of Pb^{2+}, as confirmed by X-ray Photoemission measurements, a small amount of vacancies must be utilized in order to have charge balance.

2.10. Powder X-ray diffraction

Ground single crystals of the samples were used to collect powder X-ray diffraction patterns using a PanAlytical X'Pert Pro Powder Diffractometer (Cu Kα radiation λ = 1.5418 Å) over the 2θ range of 5 - 50^0, with a step size of 0.02° and a scan speed of 0.25°/min. The measured patterns were compared to the simulated diffraction patterns using the respective single crystal data.

2.11. X-ray photoelectron spectroscopy (XPS)

X-ray photoelectron studies were performed using a Thermo Scientific ESCALAB 250 Xi spectrometer equipped with a monochromatic Al Kα X-ray source (1486.6 eV) and operated at 300 W. Samples were analyzed under vacuum ($P < 10^{-8}$ mbar), whereas survey scans and high-resolution scans were collected using pass energy of 50 eV. Binding energies were referred to the C 1s binding energy at 284.6 eV. A low-energy electron flood gun was employed for charge neutralization and ion beam etching for surface cleaning. Prior to XPS measurements, ground crystals of each sample attached on copper foil and mounted on stubs and successively put into the entry-load chamber to pump.

3. Results and discussion

3.1. Simultaneous structural transformation and partial cation exchange

In our quest to accomplishing defect engineering by design in MOCP, our group judiciously search for an MOCP system that has multiple metal cation centres with varied CE and CN in which the cation centre possesses rather labile ionic bond. The choice is made to our previously reported 1D Pb MOCP that can undergo structural change into a 3D structure with three distinctive Pb crystallographic sites fulfilling the prerequisites for multiple cation exchanges using homo- and/or aliovalent cation [63]. The 1D structure of the Pb MOCP is built around centrosymmetric Pb-dimers bridged by chloride ions. The monoprotonated ligand further connects the dimers forming a ladder-like chain extended along the *b*-axis, Fig. 1. The existence of labile chloride bridging leads to structural transformation into a 3D structure through a dissolution-recrystallization step [63]. Such a 3D compound feature three independent and crystallographically unique Pb centres, each with different CN and CE. These trinuclear independent crystallographic sites are further connected by carboxylate oxygen atoms from the ligands to form an infinite rod-like SBUs, Fig. 2, which are further linked into an extended three dimensional structure, Fig. 3 [63]. The topological analysis of the 3D structure [64] reveals a 6-nodal network with a 3,4,4,5,5,5-connected network and

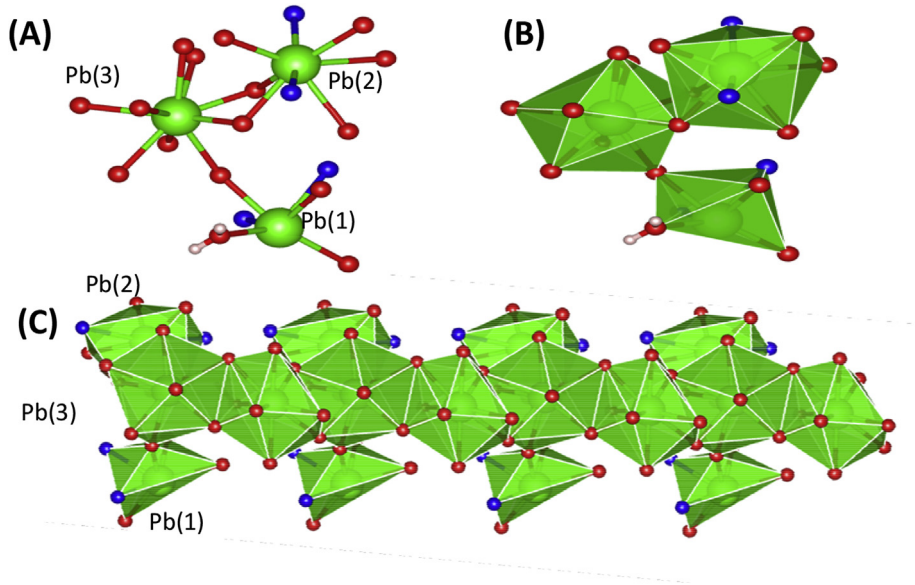

Fig. 2. Pristine 3D MOCP showing Pb^{2+} CN and CE (A), geometrical polyhedra (B), and rod-like moiety (C).

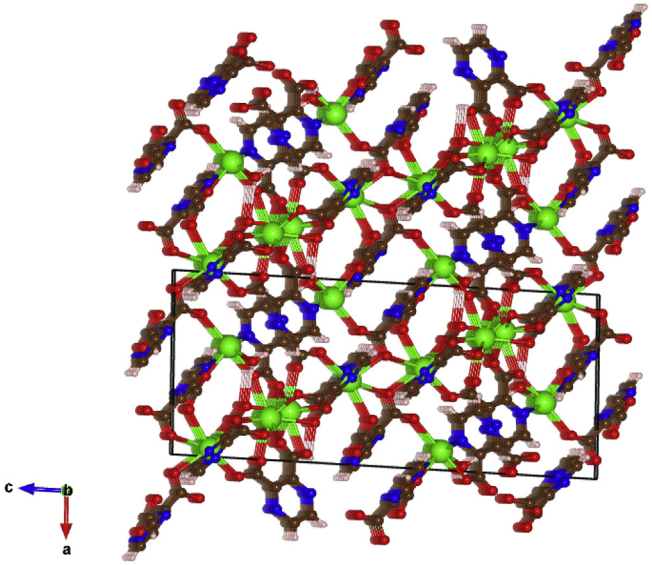

Figure 3. 3D structure of cation doped Pb^{2+} metal-organic coordination polymer (view along the *b*-axis). Green = Pb, Blue = N, Red = O, Brown = C, White = H.

stoichiometry of (3-c)(4-c)(4-c)(5-c)(5-c)(5-c).

Soaking of pure 1D Pb into different aqueous-based solutions of mono-, di-, or tri-valent cation (and their mixture), resulted in a solvent-mediated structural transformation from 1D into the 3D structure having three crystallographic distinct Pb^{2+} sites with different CN and CE, Figs. 1 and 2, that allows cationic substitutions. Similar results of dissolution-recrystallization process was observed for all of the substituted MOCPs; relatively slow (>2 h) dissolution of the 1D Pb with emergences of new crystals, the substituted MOCPs, on its surface after ~30 min of soaking and the new crystals continue to grow for 3 days to reach phase purity as confirmed by PXRD. Representative images of such processes are shown in Fig. 4.

To gain insight into how the structural transformation and cationic substitution occur, we have attempted to synthesize cation substituted Pb^{2+} MOCP directly from the known 3D structure of $Pb_3(pzdc)_3(H_2O)$, 3D Pb [65], by soaking it in similar solutions. Based on the SEM-EDS result and PXRD pattern, Fig. S1, the exogenous cation failed to dope or substitute into the 3D structure even after soaking for one month. This suggests that, the substitutional solid solution and the 3D structure may need to occur simultaneously which, in this case, can be done successfully using the dynamic, 1D Pb as starting material under suitable reaction conditions.

Li substituted Pb MOCP, Li^{+}/Pb, was successfully synthesized using a variety of Li^{+} precursors, with the largest resulting substituted crystals obtained from $LiNO_3$ precursors with the resulting formula of $Pb_{2.89}Li_{0.11}(pzdc)_3(H_2O)_{0.60}$, as refined by the single crystal X-ray diffraction, and the presence of Li, ~3.6 wt%, was confirmed by ICP-OES, Table 1, corresponding nicely to crystallographic refinement. Theoretically, monovalent substitution into divalent host, should create anion vacancy [66], however, our crystallographic refinement did not detect the presence of anion deficiency in the ligand. The PXRD pattern indicates its phase purity, Fig. S2. In this case, Li^{+} cations were found to partially substitute all the three Pb^{2+} sites with CN of 6, 7, and 9, for Pb(1), (2), and (3), respectively, Fig. 1. The latter displays two longer, hence weaker Li–O coordination bonds for O(2) and O(6), expected for smaller Li^{+}. Examples of Li-based compounds with such CNs have been reported before [67,68].

As an extension of our Co^{2+} substituted Pb MOCP, $Pb_{2.67}Co_{0.33}(pzdc)_3(H_2O)$ [58], other divalent cations with varying sizes (0.65–0.95 Å) have been successfully synthesized forming M^{2+}/Pb products, M = Co, Ni, Zn, Cd, albeit in the form of polycrystalline powders. Their PXRD patterns prove their similar structure to that of Co^{2+}/Pb and phase purity, Fig. S3. Semi-quantitative analysis of these compounds using SEM-EDS shows the presence of respective substituent in the range of 11–20 atomic %, Table 1. Due to the fact that these compounds were of similar structure to that of Co^{2+}/Pb, and the presence of respective divalent dopant was detected quantitatively, and their similar geometrical preference to that of Co^{2+} [69], we then assumed that each divalent dopant substituted at the Pb(1) sites with a similar small shift from the actual Pb(1) sites, Fig. 1, analogous to that of Co^{2+}/Pb we reported previously.

Such a shift may happen due to the absence of lone pair in these transition metal (TM) dopants, therefore giving less distorted octahedral compared to that of Pb^{2+} with its pronounced lone pair effect, Fig. S4. The preference for Pb(1) sites by exogenous TM dopants is likely due to favourable CN (i.e., six) and CE (having N and O donors including coordinated water), Fig. 2 (A) and Figure S4.

Among exogenous divalent TM cations used in here, only Cu^{2+} and Fe^{2+} did not exhibit partial cation exchange in aqueous solution, instead they both changed rapidly into known isostructures, $[M(pzdc)(H_2O)_2]\cdot 2H_2O$; M = Cu^{2+} or Fe^{2+} [70,71], facilitated by replacing bridging chloride in 1D Pb by coordinated water. Unlike the successful

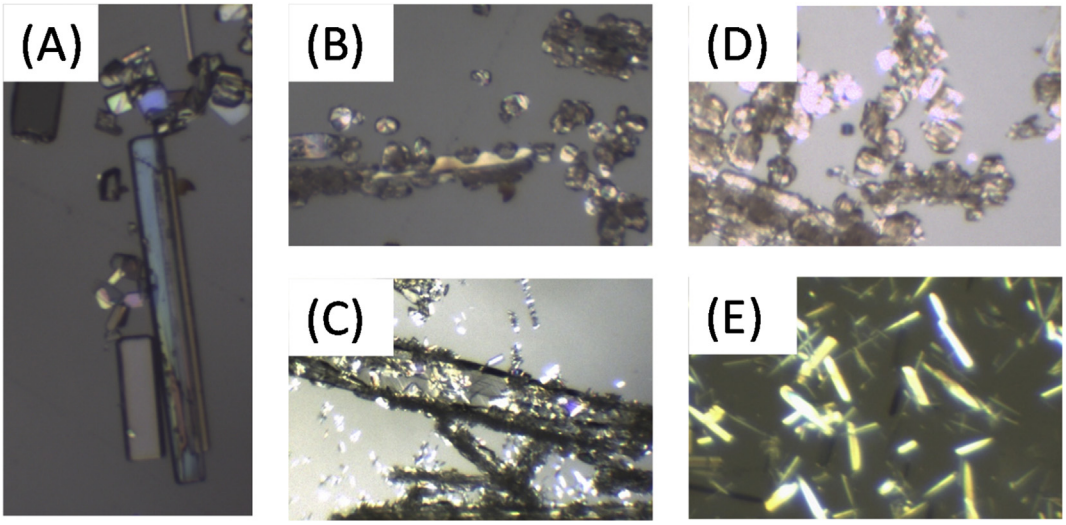

Fig. 4. Representative microscopic images of dissolution-recrystallization process: pristine 1D Pb (A); after ~30 min soaking in the aqueous solution of: Co^{2+} (B), Eu^{3+} (with or without Zn^{2+}) (C); final single crystals appearance of: Co^{2+}/Pb (D), Eu^{3+}/Pb and $Eu^{3+}/Zn^{2+}/Pb$, both have similar appearances, (E).

Table 1
SEM-EDS (average atomic %) or ICP-OES (wt.%)* results of dopant in cation doped Pb2+ metal organic coordination polymers.

Dopant	Amount (atomic or wt.%)
Li^{+}, *	3.6
Co^{2+}	11
Ni^{2+}	20
Zn^{2+}	17
Cu^{2+}	11
Cd^{2+}	12
Fe^{2+}, *	11
La^{3+}	2.0
Eu^{3+}	6.0
Gd^{3+}	6.0
Tb^{3+}	6.0
Er^{3+}	5.0
Zn^{2+}; Eu^{3+}	4.0; 1.0
Condition (1); Eu^{3+} or Tb^{3+}	6.0
Condition (2); Eu^{3+}, * or Tb^{3+}	35
Condition (3); Eu^{3+}, * or Tb^{3+}	80

substitution, in these two cases the 1D Pb dissolved relatively fast (<5 min) followed by the appearance of the new respective crystals in the solution. Through careful solvent selection based on polarity, we have successfully rendered the 1D Pb to undergo the anticipated 1D-to-3D structural transformation with a partial exchange between Pb^{2+} and Fe^{2+}, giving a doped *Fe^{2+}/Pb* product, $Pb_{2.67}Fe_{0.32}(pzdc)_3(H_2O)_{0.35}$, in which Fe^{2+} went into Pb(1) sites as expected. This was done by using an $FeCl_2$ solution of DMF/H_2O mixture (1:1 ratio), instead of a typical aqueous solution only. Its phase purity is proven by PXRD patterns, Fig. S5, with an average amount of 11 wt % of Fe^{2+} substituted into the structure, Table 1, obtained from ICP-OES. The substituted *Cu^{2+}/Pb* product was acquired by soaking the 1D Pb into a solution of Cu(II) acetate in water/DMF/1,4-dioxane, and its phase purity is shown in the PXRD pattern, Fig. S5. SEM-EDS, Table 1, confirms the presence of Cu^{2+}. In these two cases, the typical dissolution-recrystallization processes for successful doping as mentioned previously were observed.

Doping rare earth ion (Ln) into MOCPs typically endows them with long-lived luminescence, large Stokes shift, intense and tunable color emissions [72,73]. These materials are of particular importance due to their promising applications for optical sensing or solid state lighting luminescence materials [6,74,75]. Single-phase but multi-coloured emitting materials are of great importance due to their potentials for security and display applications [5,76,77]. Usually, multi-coloured emitting materials are made by incorporating Ln into the framework to form heterometallic structures which may undergo single excitation to attain dual or multiple color emission.

One of our goals is to achieve mixed valent doping. Knowing the fact that Ln^{3+} are oxophilic [78,79] and Pb(3) site is surrounded by oxygen atoms, soaking 1D Pb into Ln^{3+} aqueous solution resulted in the mixed valent substituted *Ln^{3+}/Pb* MOCP in which the Ln^{3+} went into Pb(3) oxophilic sites, in addition to Pb(1) sites. Remarkably, we found that Pb^{2+} in Pb(2) sites were fully exchanged by Ln^{3+} (La, Eu, Gd, Tb, or Er are used as representative here), Fig. 1, giving a total formula of $Pb_{2.93}La_{0.05}Vac_{0.02}(pzdc)_3(H_2O)_{0.60}$, $Pb_{2.76}Eu_{0.16}Vac_{0.08}(pzdc)_3(H_2O)_{0.56}$, $Pb_{2.73}Gd_{0.18}Vac_{0.09}(pzdc)_3(H_2O)_{0.58}$, $Pb_{2.73}Tb_{0.18}Vac_{0.09}(pzdc)_3(H_2O)_{0.60}$, and $Pb_{2.76}Er_{0.16}Vac_{0.08}(pzdc)_3(H_2O)_{0.59}$, respectively, featuring cation vacancy (Vac) on each compound. In this case, Ln are accommodated in all three Pb sites, with preference on Pb(2) sites having 7 CNs comprising O and N donors of the ligand. Due to the use of aliovalent cation substituent, cation vacancy was refined in these cases to obtain charge balances. The presence of Ln^{3+} is further proven by SEM-EDS or ICP-OES analysis, Table 1. Structural integrity of these compounds is further confirmed by PXRD, Fig. S6. The result of all Pb^{2+} sites substitutions was expected as Ln^{3+} are flexible in terms of CN and examples of Ln-based compounds with 6, 7, and 9 CNs are available [80–82].

To vary the Ln^{3+} amounts (Ln = Eu and Tb as representatives), a series of experiments were conducted by systematically exploring the effect of different synthetic conditions, considering hard soft acid base (HSAB) principle, mole ratio, pH, temperature or the reaction time. Though the details of the effects of these parameters on the structural transformation and cation exchange are still ongoing in our lab, three different synthetic conditions were applied to vary the dopant amounts: (1) an aqueous solution; (2) a mixture of three solvents (H_2O/Dioxane/DMF) with the addition of 2 drops of pyridine, while (3) is the same as (2) but with heating at 60 °C for 24 h.

In condition (1), only about 6 wt % of Ln^{3+} exchanged the Pb^{2+} ions. This is anticipated as the starting reagent, 1D Pb, tends to dissolve faster in protic solvents than aprotic ones, in addition to this, Ln^{3+} are generally hard acids and hydroxyl ions (OH^{-}) in water are hard base which, in HSAB principle, will preferentially bind and prevent Ln^{3+} ions from undergoing substitution with the host Pb^{2+}. While in conditions (2) and (3), a mixture of solvents were used, which serve to slow the transformation of 1D Pb to the 3D structure by suppressing the dissolution process of the 1D Pb and the subsequent transformation to 3D. Based on the generalized principle of HSAB, the Pb^{2+}, a borderline acid, will preferentially bind with a borderline base. Addition of 2 drops of pyridine, borderline base, into the system increases the solvation and binding of the Pb^{2+} ions by pyridine that brings it into the solution and prevents it from going back to form the 3D compound, hence, paving a way for the exogenous Ln^{3+} into the 3D structure. Using these conditions, we systematically vary the dopant amounts: 6, 35 and 80 wt% for Eu^{3+} or Tb^{3+} using conditions (1), (2), and (3), respectively. Such results give a general formula of $Pb_{3-3x}Ln_{2x}Vac_x(pzdc)_3(H_2O)$ in which x = 0.08, 0.52, and 1.2 for 6, 35, and 80 wt% of Ln (Eu^{3+} or Tb^{3+}), respectively. Note that only 6 wt% samples have been confirmed their cation vacancy (Vac) stoichiometry as refined crystallographically due to single crystallinity issue observed for other wt.% samples. The cations relative percentages are confirmed as shown in Table 1. Besides indicating phase purity and structural integrity, their Rietveld analysis of the PXRD data further shows a linear decrease in the lattice parameter *a*, with an increase in Eu^{3+} or Tb^{3+} dopant amount, which obeys the Vegard's law, Fig. 5.

A further proof-of-concept for this work was establishing hetero-valent, multiple doped MOCP, *M^{2+}/M^{3+}/Pb*. Using the chosen system, we have successfully made a hetero-valent MOCP with the resulting formula of $Pb_{2.84}Zn_{0.12}Eu_{0.02}Vac_{0.02}(pzdc)_3(H_2O)_{0.47}$, featuring cation vacancy, as refined using the single crystal X-ray diffraction data. The presence of such mixed valence and multiple doping was further supported by SEM-EDS analysis, Table 1, including EDS elemental mapping of Pb/Zn/Eu, Fig. S7. PXRD pattern, Fig. S8, shows its phase purity and structural integrity. We found that Eu^{3+} and Zn^{2+} were substituted into Pb(1) sites, with the latter occupies a slightly shifted position to that of Pb(1) site as expected. Pb(2) and (3) sites were found unsubstituted. Zn^{2+} preference to exchange at Pb(1) is anticipated, consistent with its single dopant counterpart (*Zn^{2+}/Pb*). Eu^{3+} choice of site, however, is rather unexpected since its single dopant counterpart (*Eu^{3+}/Pb*) preferred Pb(2) site as it underwent full exchange, from Pb^{2+} into Eu^{3+}, in this site. Understanding the substitution mechanism and site preferences as well as the reason for deficient water stoichiometry that may have to do with vacancy formation requires further investigations.

3.2. XPS results

Eu^{3+}/Pb, *Eu^{3+}/Zn^{2+}/Pb*, *Li^{+}/Pb*, and *Fe^{2+}/Pb* were characterized by XPS as representative doped products to investigate their oxidation state and CE, Fig. S9. The splitting of the binding energy of 4*f* orbitals in Pb and the energies of the 3*d* orbitals for Eu are attributed to the strong spin-orbit coupling. The binding energy of Pb 4*f* is assigned as 143.3 ($4f_{5/2}$) and 138.4 ($4f_{7/2}$) eV which is consistent with +2 oxidation states of Pb [83]. The very similar binding energies of Pb in these MOCPs are indicative for their very similar CE. The binding energies of Eu in *Eu^{3+}/Pb*, and *Zn^{2+}/Eu^{3+}/Pb* are at 1125.1 ($3d_{5/2}$) and 1135.2 ($3d_{3/2}$). The binding energies at 1022.5eV and 710.2eV correspond to the Zn ($2p_{3/2}$) and Fe ($2p_{3/2}$) orbitals in *Eu^{3+}/Zn^{2+}/Pb* and *Fe^{2+}/Pb*, respectively

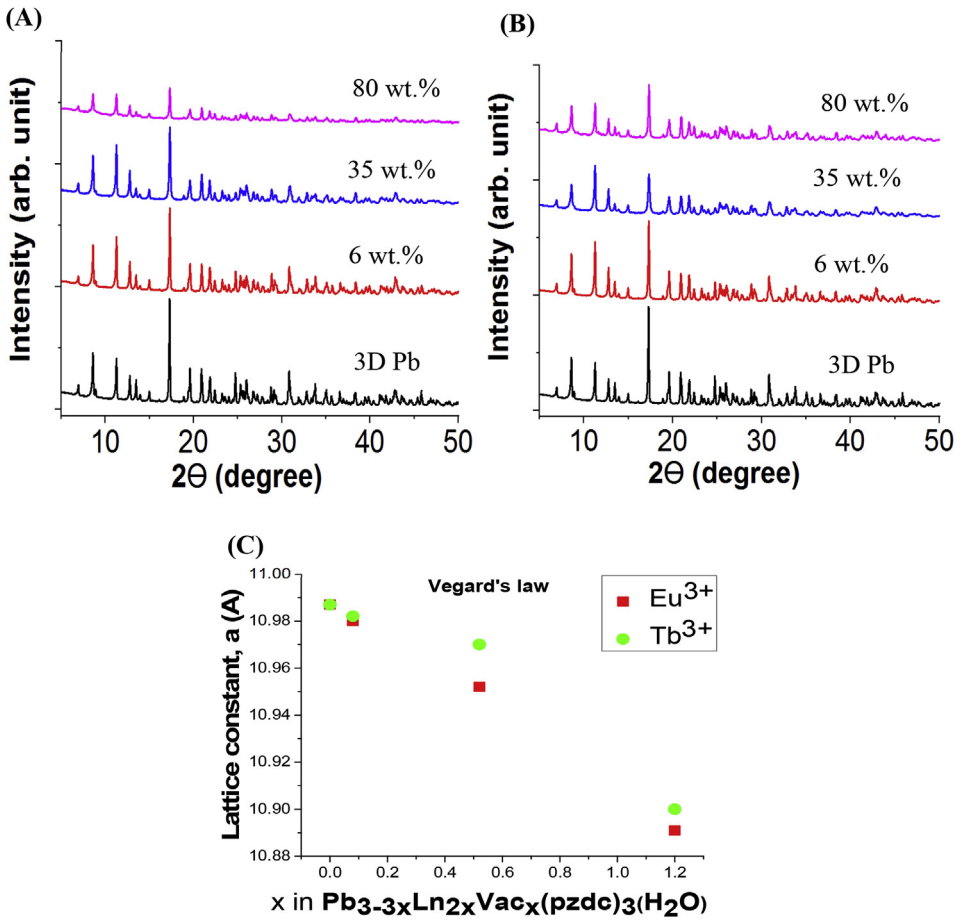

Fig. 5. PXRD patterns of: (A) *Eu^{3+}/Pb* with 6, 35 and 80 wt % of Eu^{3+}, and (B) *Tb^{3+}/Pb* with 6, 35 and 80 wt % of Tb^{3+}. (C) Rietveld refinements of powder X-ray diffraction data with incorporation of smaller Eu^{3+} or Tb^{3+} (note that the stoichiometry, x, corresponds to 6, 35, and 80 wt% of the dopant).

[83]. Li^+ in *Li^+/Pb* was not detected by XPS because the Li concentration was very low and below the detection limit. Presence of Li was determined indirectly by single crystal X-ray diffraction, where the occupancy of Pb atoms which share the same site with Li was refined. The resulting Li/Pb stoichiometric ratio was validated by ICP-OES.

3.3. Photoluminescence

Based on the *Laporte* selection rule, the low absorption and the forbidden nature of the *f-f* transitions are inherent property of most Ln^{3+} ions which make them less efficient light energy absorbers [84]. To overcome the poor light absorption, Ln^{3+} are typically introduced into a system with suitable organic chromophore that can efficiently absorb energy and transfer to the Ln^{3+} ions, the so-called *antennae effect*.

A photoluminescence evaluation was conducted on Ln substituted Pb MOCP, namely *Eu^{3+}/Pb*, *Tb^{3+}/Pb*, and *Eu^{3+}/Zn^{2+}/Pb*. At ~6 wt% of Eu^{3+} or Tb^{3+} doping, was enough to tune its photoluminescence from weak greenish yellow emission (original undoped Pb 3D) with CIE coordinate of (0.38, 0.58), to bright yellowish red (*Eu^{3+}/Pb)* that corresponds to CIE coordinate of (0.35, 0.37); while adding extra dopant, Zn^{2+}, to make *Eu^{3+}/Zn^{2+}/Pb* leads to yellowish orange luminescence color with CIE coordinate of (0.36, 0.42). Bright greenish yellow was observed for *Tb^{3+}/Pb* with CIE coordinate of (0.38, 0.48), Fig. S10. Such results suggest a good antennae effect, especially in the case of *Eu^{3+}/Pb* where typical Eu^{3+} *f-f* transitions were observed [85]. Interestingly, the PL character of original 3D Pb host, a broad emission peaked at greenish yellow, is sustained within the background, making this compound as a dual color luminescence under single-excitation wavelength (473 nm). However, this may indicate the absorbed energy by the organic ligands was only partly transferred to the Eu^{3+} or Tb^{3+}.

The efficiency of the energy transfer was improved, thus better antennae effect, when the excitation wavelength was increased to 350 nm. The broad peak of the pristine 3D Pb-host disappeared indicating a more efficient energy transfer within the framework. In this case, only the characteristic peaks of Eu^{3+} *f-f* transitions ($^5D_0 \rightarrow {}^7F_j$, j = 0–4) and that of Tb^{3+} ($^5D_4 \rightarrow {}^7F_j$, j = 3–6) were observed, Fig. 6(A) and (B), respectively. Observation of LMCT, as indicated by blue-shifting of the ligand's 260 nm band in Eu^{3+}/Pb and Tb^{3+}/Pb in solid state UV–Vis absorption Figures S11 (A) and (B), support the observed antennae effect.

A decrease of PL intensity is typically observed in a doping system with 10–20% dopant, hindering the solid state lighting efficiency [86,87]. There are reports, however, that show an increase in PL intensity at higher dopant amount (>20%) which depends on synthetic pathway adopted that leads to the absence of dopant cluster formation, i.e. homogeneous dopant distribution, reducing PL quenching that occurs due to cross relaxation [86,87].

Eyeing for enhancing the PL efficiency, we further investigate the solid state PL emission of as synthesized 6, 35 and 80 wt % of Eu^{3+} or Tb^{3+} doped compounds, successfully engineered using the three aforementioned synthetic conditions. Excited at 350 nm, both Eu^{3+} and Tb^{3+} doped compounds show only their expected characteristic *f-f* transition peaks. Eu^{3+} doped compounds show a remarkable increase in PL intensity when the dopant amount increases, Fig. 6 (A), which may suggest the lack of Eu^{3+} clusters formation that can trigger cross relaxation resulting in PL quenching [86,87].

The fact that partial cation substitutions in this system occurred onto three crystallographically distinct Pb^{2+} sites, well separated by the ligand, may support the argument that such cluster formation of dopants

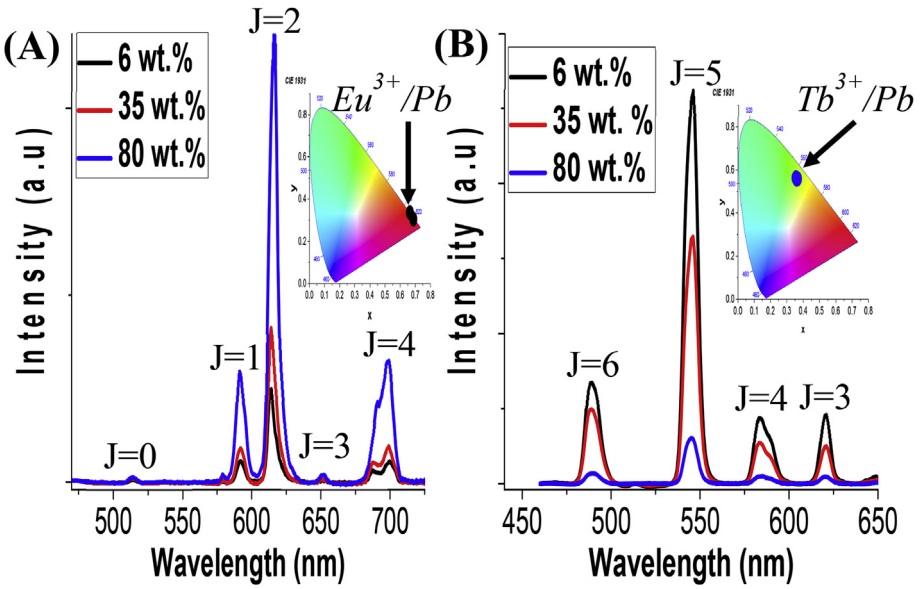

Fig. 6. Solid-state photoluminescence (emission) spectra of Eu^{3+}/Pb with 6, 35 and 80 wt% of Eu^{3+} (A), and Tb^{3+}/Pb with 6, 35 and 80 wt% of Tb^{3+} (B). The insets are their CIE chromaticity diagrams.

may diminished or at least be minimized. However, in the case of Tb^{3+}, while displaying typical Tb^{3+} characteristic peaks, the peak intensity decreases as the dopant amount increases, Fig. 6 (B), interestingly, without total PL quenching. This supports the argument above that the dopant cluster formation, in the case of Tb^{3+}, may at least be minimized, hence total PL quenching is not observed. Figure S12 (A) and (B) shows the corresponding digital images of the Eu^{3+} and Tb^{3+} doped with 6, 35 and 80 wt % under 365 nm UV lamp.

Intrigued by the fact that Eu^{3+}/Pb system exhibited a PL intensity increase up to 80 wt% doping as well as a dual color luminescence, attempts to orchestrate multiple colours luminescence spanning from UV, visible, to NIR are currently underway in our laboratory through judicious selection of Ln dopant(s) with variable amount. PL color tuning to achieve white emission, including theoretical investigations on PL mechanism in this system are also under investigation.

4. Conclusion

In summary, Pb MOCP solid solutions featuring mixed valence, cation vacancy and multiple substitutions have been successfully synthesized using a 1D model MOCP that leads to a 3D system with crystallographically different Pb^{2+} sites with different coordination numbers and atomic environments that allow them to be substituted with variety of cations of different valences and sizes, under appropriate conditions. Simultaneous structural change (1D to 3D) and cationic substitution seem to be the pathway for making the solid solutions. The photoluminescence study showed that this system has potential as a tunable luminescent color material with increased intensity even up to 80 wt% Eu^{3+} doping, the first in luminescing MOCP, to the best of our knowledge. Such a result is promising and deemed for further investigations to achieve higher light efficiency in solid state lighting application.

Acknowledgment

Financial supports for this research were provided by HIR Chancellory Grant UM.C/625/1/HIR/211 from the University of Malaya and Fundamental Research Grant Scheme, Ministry of Education, Malaysia, Project No. FP 037-2014A. ACW would like to thank A. Rahman Yusoff, M. Fauzan Zainudin and M. Shukri Ab. Aziz of Chemistry, Univ. of Malaya for PXRD and SEM-EDS measurements. ACW also thanks Fauzan Rezki, Sunardi Rahman, and Siti Amira M. Hussin for doing some syntheses and characterizations. The single crystal X-ray work made use of the IMSERC at Northwestern University, which has received support from the Soft and Hybrid Nanotechnology Experimental (SHyNE) Resource (NSF NNCI-1542205); the State of Illinois and International Institute for Nanotechnology (IIN).

Appendix A. Supplementary data

Supplementary data to this article can be found online at https://doi.org/10.1016/j.jssc.2019.120948.

References

[1] C.-Y. Sun, X.-L. Wang, X. Zhang, C. Qin, P. Li, Z.-M. Su, D.-X. Zhu, G.-G. Shan, K.-Z. Shao, H. Wu, J. Li, Efficient and tunable white-light emission of metal–organic frameworks by iridium-complex encapsulation, Nat. Commun. 4 (2013).
[2] X. Mi, D. Sheng, Y.e. Yu, Y. Wang, L. Zhao, J. Lu, Y. Li, D. Li, J. Dou, J. Duan, Tunable light emission and multiresponsive luminescent sensitivities in aqueous solutions of two series of lanthanide metal–organic frameworks based on structurally related ligands, Acs Appl. Mater. Inter. 11 (2019) 7914–7926.
[3] H.E. Emam, H.N. Abdelhamid, R.M. Abdelhameed, Self-cleaned photoluminescent viscose fabric incorporated lanthanide-organic framework (Ln-MOF), Dyes Pigments 159 (2018) 491–498.
[4] X.-P. Zhang, D.-G. Wang, Y. Su, H.-R. Tian, J.-J. Lin, Y.-L. Feng, J.-W. Cheng, Luminescent 2D bismuth–cadmium–organic frameworks with tunable and white light emission by doping different lanthanide ions, Dalton Trans. 42 (2013) 10384–10387.
[5] R. An, H. Zhao, H.-M. Hu, X. Wang, M.-L. Yang, G. Xue, Synthesis, structure, white-light emission, and temperature recognition properties of Eu/Tb mixed coordination polymers, Inorg. Chem. 55 (2016) 871–876.
[6] X.-Y. Xu, B. Yan, Eu(III)-Functionalized MIL-124 as fluorescent probe for highly selectively sensing ions and organic small molecules especially for Fe(III) and Fe(II), ACS Appl. Mater. Interfaces 7 (2015) 721–729.
[7] S. Kempahanumakkagari, K. Vellingiri, A. Deep, E.E. Kwon, N. Bolan, K.H. Kim, Metal-organic framework composites as electrocatalysts for electrochemical sensing applications, Coord. Chem. Rev. 357 (2018) 105–129.
[8] H.L. Wang, Q.L. Zhu, R.Q. Zou, Q. Xu, Metal-organic frameworks for energy applications, Chem-Us 2 (2017) 52–80.
[9] H.E. Emam, A.E. Abdelhamid, R.M. Abdelhameed, Refining of liquid fuel from N-Containing compounds via using designed Polysulfone@ Metal organic framework composite film, J. Clean. Prod. 218 (2019) 347–356.
[10] R.M. Abdelhameed, H.E. Emam, Design of ZIF (Co & Zn)@ wool composite for efficient removal of pharmaceutical intermediate from wastewater, J. Colloid Interface Sci. 552 (2019) 494–505.
[11] R.M. Abdelhameed, M. Rehan, H.E. Emam, Figuration of Zr-based MOF@ cotton fabric composite for potential kidney application, Carbohydr. Polym. 195 (2018) 460–467.
[12] R.M. Abdelhameed, H.R. el-deib, F.M. El-Dars, H.B. Ahmed, H.E. Emam, Applicable strategy for removing liquid fuel nitrogenated contaminants using MIL-53-NH2@ natural fabric composites, Ind. Eng. Chem. Res. 57 (2018) 15054–15065.

[13] R.M. Abdelhameed, H.E. Emam, J. Rocha, A.M. Silva, Cu-BTC metal-organic framework natural fabric composites for fuel purification, Fuel Process. Technol. 159 (2017) 306–312.
[14] R.M. Abdelhameed, H. Abdel-Gawad, M. Elshahat, H.E. Emam, Cu–BTC@ cotton composite: design and removal of ethion insecticide from water, RSC Adv. 6 (2016) 42324–42333.
[15] J.M. Taylor, S. Dekura, R. Ikeda, H. Kitagawa, Defect control to enhance proton conductivity in a metal–organic framework, Chem. Mater. 27 (2015) 2286–2289.
[16] W. Liang, C.J. Coghlan, F. Ragon, M. Rubio-Martinez, D.M. D'Alessandro, R. Babarao, Defect engineering of UiO-66 for CO2 and H2O uptake - a combined experimental and simulation study, Dalton Trans. 45 (2016) 4496–4500.
[17] G.C. Shearer, S. Chavan, S. Bordiga, S. Svelle, U. Olsbye, K.P. Lillerud, Defect engineering: tuning the porosity and composition of the metal–organic framework UiO-66 via modulated synthesis, Chem. Mater. 28 (2016) 3749–3761.
[18] Z. Fang, B. Bueken, D.E. De Vos, R.A. Fischer, Defect-engineered metal-organic frameworks, Angew. Chem. Int. Ed. 54 (2015) 7234–7254.
[19] A.K. Cheetham, T.D. Bennett, F.X. Coudert, A.L. Goodwin, Defects and disorder in metal organic frameworks, Dalton Trans. 45 (2016) 4113–4126.
[20] C.A. Trickett, K.J. Gagnon, S. Lee, F. Gandara, H.B. Burgi, O.M. Yaghi, Definitive molecular level characterization of defects in UiO-66 crystals, Angew. Chem. Int. Ed. 54 (2015) 11162–11167.
[21] P. Capper, Bulk Crystal Growth in Electronic, Optical, and Optoelectronic Materials, Wiley, New York, 2005.
[22] J. Singh, Electronic and Optoelectronic Properties of Semiconductor Structures, Cambridge University Press, Cambridge, 2003.
[23] L.M. Aguirre-Diaz, F. Gandara, M. Iglesias, N. Snejko, E. Gutierrez-Puebla, M.A. Monge, Tunable catalytic activity of solid solution metal-organic frameworks in one-pot multicomponent reactions, J. Am. Chem. Soc. 137 (2015) 6132–6135.
[24] S.R. Batten, D.R. Turner, M.S. Neville, Coordination Polymers: Design, Analysis and Application, RSC, Cambridge, 2009.
[25] S. Chaemchuem, Z. Kui, F. Verpoort, Control of interpenetration via in situ lithium incorporation in MOFs and their gas adsorption properties and selectivity, CrystEngComm 18 (2016) 7614–7619.
[26] Z. Fang, J.P. Durholt, M. Kauer, W. Zhang, C. Lochenie, B. Jee, B. Albada, N. Metzler-Nolte, A. Poppl, B. Weber, M. Muhler, Y. Wang, R. Schmid, R.A. Fischer, Structural complexity in metal-organic frameworks: simultaneous modification of open metal sites and hierarchical porosity by systematic doping with defective linkers, J. Am. Chem. Soc. 136 (2014) 9627–9636.
[27] H. Furukawa, U. Muller, O.M. Yaghi, Heterogeneity within order" in metal-organic frameworks, Angew. Chem. Int. Ed. 54 (2015) 3417–3430.
[28] S. Horike, D. Umeyama, S. Kitagawa, Ion conductivity and transport by porous coordination polymers and metal-organic frameworks, Acc. Chem. Res. 46 (2013) 2376–2384.
[29] H.C. Zhou, S. Kitagawa, Metal-organic frameworks (MOFs), Chem. Soc. Rev. 43 (2014) 5415–5418.
[30] S. Kitagawa, R. Kitaura, S. Noro, Functional porous coordination polymers, Angew. Chem. Int. Ed. 43 (2004) 2334–2375.
[31] O. Kozachuk, I. Luz, F.X. Llabres i Xamena, H. Noei, M. Kauer, H.B. Albada, E.D. Bloch, B. Marler, Y. Wang, M. Muhler, R.A. Fischer, Multifunctional, defect-engineered metal-organic frameworks with ruthenium centers: sorption and catalytic properties, Angew. Chem. Int. Ed. 53 (2014) 7058–7062.
[32] O. Kozachuk, M. Meilikhov, K. Yusenko, A. Schneemann, B. Jee, A.V. Kuttatheyil, M. Bertmer, C. Sternemann, A. Pöppl, R.A. Fischer, A solid-solution approach to mixed-metal metal-organic frameworks - detailed characterization of local structures, defects and breathing behaviour of Al/V frameworks, Eur. J. Inorg. Chem. 2013 (2013) 4546–4557.
[33] Y. Liu, R.C. Klet, J.T. Hupp, O. Farha, Probing the correlations between the defects in metal-organic frameworks and their catalytic activity by an epoxide ring-opening reaction, Chem. Commun. 52 (2016) 7806–7809.
[34] P. Ramaswamy, N.E. Wong, G.K. Shimizu, MOFs as proton conductors–challenges and opportunities, Chem. Soc. Rev. 43 (2014) 5913–5932.
[35] L. Sun, M.G. Campbell, M. Dinca, Electrically conductive porous metal-organic frameworks, Angew. Chem. Int. Ed. 55 (2016) 3566–3579.
[36] Y. Chuan Tan, H. Chun Zeng, Self-templating synthesis of hollow spheres of MOFs and their derived nanostructures, Chem. Commun. 52 (2016) 11591–11594.
[37] C.H. Hendon, D. Tiana, A. Walsh, Conductive metal-organic frameworks and networks: fact or fantasy? Phys. Chem. Chem. Phys. 14 (2012) 13120–13132.
[38] F. Gul-E-Noor, B. Jee, M. Mendt, D. Himsl, A. Poppl, M. Hartmann, J. Haase, H. Krautscheid, M. Bertmer, formation of mixed metal Cu3-xZnx(btc)(2) frameworks with different zinc contents: incorporation of Zn2+ into the metal-organic framework structure as studied by solid-state NMR, J. Phys. Chem. C 116 (2012) 20866–20873.
[39] Y. Jiao, C.R. Morelock, N.C. Burtch, W.P. Mounfield, J.T. Hungerford, K.S. Walton, Tuning the kinetic water stability and adsorption interactions of Mg-MOF-74 by partial substitution with Co or Ni, Ind. Eng. Chem. Res. 54 (2015) 12408–12414.
[40] O. Kozachuk, K. Khaletskaya, M. Halbherr, A. Betard, M. Meilikhov, R.W. Seidel, B. Jee, A. Poppl, R.A. Fischer, Microporous mixed-metal layer-pillared [Zn1-xCux(bdc)(dabco)0.5] MOFs: preparation and characterization, Eur. J. Inorg. Chem. 2012 (2012) 1688–1695.
[41] M.V. Parkes, D.F. Sava Gallis, J.A. Greathouse, T.M. Nenoff, Effect of metal in M3(btc)2and M2(dobdc) MOFs for O2/N2Separations: a combined density functional theory and experimental study, J. Phys. Chem. C 119 (2015) 6556–6567.
[42] B. Tu, Q. Pang, D. Wu, Y. Song, L. Weng, Q. Li, Ordered vacancies and their chemistry in metal-organic frameworks, J. Am. Chem. Soc. 136 (2014) 14465–14471.
[43] G.T. Vuong, M.H. Pham, T.O. Do, Synthesis and engineering porosity of a mixed metal Fe2Ni MIL-88B metal-organic framework, Dalton Trans. 42 (2013) 550–557.
[44] W. Zhang, Z. Chen, M. Al-Naji, P. Guo, S. Cwik, O. Halbherr, Y. Wang, M. Muhler, N. Wilde, R. Glaser, R.A. Fischer, Simultaneous introduction of various palladium active sites into MOF via one-pot synthesis: Pd@[Cu3-xPdx(BTC)2]n, Dalton Trans. 45 (2016) 14883–14887.
[45] V. Nikas, N. Tabassum, B. Ford, L. Smith, A.E. Kaloyeros, S. Gallis, Strong visible light emission from silicon-oxycarbide nanowire arrays prepared by electron beam lithography and reactive ion etching, J. Mater. Res. 30 (2015) 3692–3699.
[46] R.E. Brandt, J.R. Poindexter, P. Gorai, R.C. Kurchin, R.L. Hoye, L. Nienhaus, M.W. Wilson, J.A. Polizzotti, R. Sereika, R. Žaltauskas, Searching for "defect-tolerant" photovoltaic materials: combined theoretical and experimental screening, Chem. Mater. 29 (2017) 4667–4674.
[47] D.H. Fabini, J.G. Labram, A.J. Lehner, J.S. Bechtel, H.A. Evans, A. Van der Ven, F. Wudl, M.L. Chabinyc, R. Seshadri, Main-group halide semiconductors derived from perovskite: distinguishing chemical, structural, and electronic aspects, Inorg. Chem. 56 (2016) 11–25.
[48] G. Laurita, D.H. Fabini, C.C. Stoumpos, M.G. Kanatzidis, R. Seshadri, Chemical tuning of dynamic cation off-centering in the cubic phases of hybrid tin and lead halide perovskites, Chem. Sci. 8 (2017) 5628–5635.
[49] C.K. Brozek, M. Dinca, Cation exchange at the secondary building units of metal-organic frameworks, Chem. Soc. Rev. 43 (2014) 5456–5467.
[50] G.G. Briand, N. Burford, Coordination complexes of bismuth(III) involving organic ligands with pnictogen or chalcogen donors, Adv. Inorg. Chem. 50 (2000) 285–357.
[51] R.G. Pearson, Hard and soft acids and bases, J. Am. Chem. Soc. 85 (1963) 3533–3539.
[52] K.P. Rao, A. Thirumurugan, C.N. Rao, Lamellar and three-dimensional hybrid compounds formed by cyclohexene- and cyclohexanedicarboxylates of Pb, La, and Cd, Chem. Eur J. 13 (2007) 3193–3201.
[53] A. Thirumurugan, R.A. Sanguramath, C.N. Rao, Hybrid structures formed by lead 1,3-cyclohexanedicarboxylates, Inorg. Chem. 47 (2008) 823–831.
[54] S.R. Fan, L.G. Zhu, Syntheses, structures, and characterizations of four new lead(II) 5-sulfosalicylate complexes with both chelating and bridging neutral ligands, Inorg. Chem. 46 (2007) 6785–6793.
[55] J. Yang, G.D. Li, J.J. Cao, Q. Yue, G.H. Li, J.S. Chen, Structural variation from 1D to 3D: effects of ligands and solvents on the construction of lead(II)-organic coordination polymers, Chem. Eur J. 13 (2007) 3248–3261.
[56] J. Yang, J.-F. Ma, Y.-Y. Liu, J.-C. Ma, S.R. Batten, A series of lead(II) complexes with π−π stackings: structural diversities by varying the ligands, Cryst. Growth Des. 9 (2009) 1894–1911.
[57] Y.H. Zhao, H.B. Xu, Y.M. Fu, K.Z. Shao, S.Y. Yang, Z.M. Su, X.R. Hao, D.X. Zhu, E.B. Wang, A series of lead(II)-Organic frameworks based on pyridyl carboxylate acid N-oxide derivatives: syntheses, structures, and luminescent properties, Cryst. Growth Des. 8 (2008) 3566–3576.
[58] F.Y. Wardana, S.-W. Ng, A.C. Wibowo, The lead coordination polymers containing pyrazine-2,3-dicarboxylic acid: rapid structural transformations and cation exchange, Cryst. Growth Des. 15 (2015) 5930–5938.
[59] S. Zhang, Q. Wei, G. Xie, Q. Yang, S.P. Chen, In situ hydrothermal syntheses, structures and photoluminescent properties of three coordination polymers based on 3-amidecarbonylpyrazine-2-carboxylic acid, Inorg. Chim. Acta 387 (2012) 52–57.
[60] S. Bruker, Saint, Bruker AXS Inc., Madison, Wisconsin, USA, 2002.
[61] O.V. Dolomanov, L.J. Bourhis, R.J. Gildea, J.A.K. Howard, H. Puschmann, OLEX2: a complete structure solution, refinement and analysis program, J. Appl. Crystallogr. 42 (2009) 339–341.
[62] G. Sheldrick, A short history of SHELX, Acta Crystallogr. A 64 (2008) 112–122.
[63] F.Y. Wardana, S.W. Ng, A.C. Wibowo, The lead coordination polymers containing pyrazine-2,3-dicarboxylic acid: rapid structural transformations and cation exchange, Cryst. Growth Des. 15 (2015) 5930–5938.
[64] V.A. Blatov, Multipurpose crystallochemical analysis with the program package TOPOS, IUCr CompComm Newslett. 7 (2006) 4–38.
[65] S. Zhang, Q. Wei, G. Xie, Q. Yang, S. Chen, In situ hydrothermal syntheses, structures and photoluminescent properties of three coordination polymers based on 3-amidecarbonylpyrazine-2-carboxylic acid, Inorg. Chim. Acta 387 (2012) 52–57.
[66] A.R. West, Solid State Chemistry and its Applications, John Wiley & Sons, 2014.
[67] A.F. Holleman, E. Wiberg, N. Wiberg, Inorganic Chemistry, Academic Press, 2001.
[68] G.R. Redhammer, G. Roth, Lithium and sodium yttrium orthosilicate oxyapatite, LiY9(SiO4)6O2, at both 100 K and near room temperature, Acta Crystallogr. C 59 (2003) 120–124.
[69] J.A.S. Howell, P.M. Burkinshaw, Ligand substitution reactions at low-valent four-, five-, and six-coordinate transition metal centers, Chem. Rev. 83 (1983) 557–599.
[70] L. Mao, S.J. Rettig, R.C. Thompson, J. Trotter, S. Xia, 2, 3-Pyrazinedicarboxylates of cobalt (II), nickel (II), and copper (II); magnetic properties and crystal structures, Can. J. Chem. 74 (1996) 433–444.
[71] H. Xu, H. Ma, M. Xu, W. Zhao, B. Guo, catena-Poly [[[diaquairon (II)]-μ-pyrazine-2, 3-dicarboxylato] dihydrate], Acta Crystallogr. 64 (2008) m104-m104.
[72] Y. Cui, Y. Yue, G. Qian, B. Chen, Luminescent functional metal–organic frameworks, Chem. Rev. 112 (2012) 1126–1162.
[73] Z. Hu, B.J. Deibert, J. Li, Luminescent metal–organic frameworks for chemical sensing and explosive detection, Chem. Soc. Rev. 43 (2014) 5815–5840.
[74] Y. Lu, B. Yan, Lanthanide organic–inorganic hybrids based on functionalized metal–organic frameworks (MOFs) for a near-UV white LED, Chem. Commun. 50 (2014) 15443–15446.

[75] Y. Zhou, B. Yan, F. Lei, Postsynthetic lanthanide functionalization of nanosized metal–organic frameworks for highly sensitive ratiometric luminescent thermometry, Chem. Commun. 50 (2014) 15235–15238.
[76] Q.-Y. Yang, M. Pan, S.-C. Wei, K. Li, B.-B. Du, C.-Y. Su, Linear dependence of photoluminescence in mixed ln-MOFs for color tunability and barcode application, Inorg. Chem. 54 (2015) 5707–5716.
[77] Z.-F. Liu, M.-F. Wu, S.-H. Wang, F.-K. Zheng, G.-E. Wang, J. Chen, Y. Xiao, A.-Q. Wu, G.-C. Guo, J.-S. Huang, Eu 3+-doped Tb 3+ metal–organic frameworks emitting tunable three primary colors towards white light, J. Mater. Chem. C 1 (2013) 4634–4639.
[78] K.P. Kepp, A quantitative scale of oxophilicity and thiophilicity, Inorg. Chem. 55 (2016) 9461–9470.
[79] J.W. Steed, J.L. Atwood, Supramolecular Chemistry, John Wiley & Sons, Ltd., UK, 2009.
[80] J.D. Einkauf, J.M. Clark, A. Paulive, G.P. Tanner, D.T. de Lill, A general model of sensitized luminescence in lanthanide-based coordination polymers and metal-organic framework materials, Inorg. Chem. 56 (2017) 5544–5552.
[81] D.G. Karraker, Hypersensitive transitions of six-, seven-, and eight-coordinate neodymium, holmium, and erbium chelates, Inorg. Chem. 6 (1967) 1863–1868.
[82] J.-C.G. Bunzli, Review: lanthanide coordination chemistry: from old concept to coordination polymers, J. Coord. Chem. 67 (2014) 3706–3733.
[83] A.Y. Lee, D.M. Blakeslee, C.J. Powell, J.R. Rumble, The NIST X-Ray Photoelectron Spectroscopy (XPS) Database, 2012.
[84] F.J. Steemers, W. Verboom, D.N. Reinhoudt, E.B. van der Tol, J.W. Verhoeven, New sensitizer-modified calix[4]arenes enabling near-UV excitation of complexed luminescent lanthanide ions, J. Am. Chem. Soc. 117 (1995) 9408–9414.
[85] Y.J. Cui, Y.F. Yue, G.D. Qian, B.L. Chen, Luminescent functional metal-organic frameworks, Chem. Rev. 112 (2012) 1126–1162.
[86] J.-C.G. Bünzli, Lanthanide coordination chemistry: from old concepts to coordination polymers, J. Coord. Chem. 67 (2014) 3706–3733.
[87] B. Ritter, P. Haida, F. Fink, T. Krahl, K. Gawlitza, K. Rurack, G. Scholz, E. Kemnitz, Novel and easy access to highly luminescent Eu and Tb doped ultra-small CaF2, SrF2 and BaF2 nanoparticles – structure and luminescence, Dalton Trans. 46 (2017) 2925–2936.